The Effect of Building Direction on Microstructure and Microhardness during Selective Laser Melting of Ti6Al4V Titanium Alloy

D. Palmeri, G. Buffa, G. Pollara, and L. Fratini

During the last few years, additive manufacturing has been more and more extensively used in several industries, especially in the aerospace and medical device fields, to produce Ti6Al4V titanium alloy parts. During the Selective Laser Melting (SLM) process, the heterogeneity of finished product is strictly connected to the scan strategies and the building direction. An optimal managing of the latter parameters allows to better control and defines the final mechanical and metallurgical properties of parts. Acting on the building direction it is also possible to optimize the critical support structure. In particular, more support structures are needed for the sample at 0°, while very low support are required for the sample at 90°. To study the effects of build direction on microstructure heterogeneity evolution and mechanical performances of selective laser melted Ti6Al4V parts, two build direction samples (0°, 90°) were manufactured and analyzed using optical metallographic microscope (OM) and scanning electron microscopy (SEM). Isometric microstructure reconstruction and microhardness tests were carried out in order to analyze the specimens. The obtained results indicate that the build direction has to be considered a key geometrical parameter affecting the overall quality of the obtained products.

1. Introduction

Additive manufacturing (AM) technologies are increasingly widespread in the production of metal components used in various engineering sectors because the significant advantages related to the possibility to obtain complex geometries, difficult to achieve with other technologies, together with the reduction in production waste, energy costs and assembly costs (Ref 1). Although there are significant advantages associated with additive manufacturing technologies, it should be considered that there are also a few shortcomings, related to the fact that the production phases result in strong thermal gradients and high cooling rates that give rise to thermal stresses, phase segregation phenomena and the development of metastable phases. Such phenomena cause microstructural anisotropies which in turn produce anisotropies of mechanical properties in the final piece. The in-depth study of the links between process parameters, microstructure, and final mechanical properties of parts produced by AM is therefore strategic

for the further development of this production technique (Ref 2).

The main technologies used in the additive manufacture of metal components can be divided into those involving the material melting and those involving the material sintering and melting. Among the first group there are: the laser-powder bed fusion (L-PBF) technology, in the following referred as Selective Laser Melting (SLM), where selective fusion of areas of a powder metal bed are obtained using a laser beam as a heat source (Ref 3, 4); the electron beam melting (EBM) technology, where selective fusion of areas of a powder metal bed are obtained using an electronic beam as a heat source (Ref 5, 6); the Direct Energy Deposition (DED) technology, where material deposition is obtained through local melting of wires or metal powders (Ref 7, 8). Among the second group there are: the metal binder jetting (MBJ) technology, where a metal powder consolidated using a polymer binder, subsequently chemically or thermally eliminated, is then sintered through an appropriate heat treatment; the fused filament fabrication (FFF) technology, where the deposition of a wire composed of metal powder and a polymer binder undergoes to the same steps indicated for Binder Jetting technology (Ref 9).

These technologies are suitable to various types of metal alloys, being among the most used aluminum alloys (Al-Si10Mg), titanium alloys (Ti6Al4V), Chromium-Cobalt alloys, stainless steel (AISI 316L) and nickel alloys (Inconel 718) frequently used in the automotive, aerospace and industrial automation sectors as well as in the medical field (Ref 10, 11). Recent trends include also AlNiCu aluminum alloys for the fabrication of High-Fracture-Resistance alloys (Ref 12) and nickel alloys (NiTi, NiTiHf) for the fabrication of shape memory alloys (Ref 13,14) used for automotive and medical application, respectively.

AM technologies involve repeated melting and rapid solidification of material, coupled with solid state phase

D. Palmeri, G. Buffa, G. Pollara, and **L. Fratini**, Department of Engineering, University of Palermo, Viale delle Scienze, 90128 Palermo, Italy. Contact e-mail: gianluca.buffa@unipa.it.

transformations and directional heat flows (Ref 15). These factors determine both heterogeneity, as pores due to trapped gas in the powder bed and pores caused by insufficient melting (Ref 16), and anisotropy in microstructural evolutions, grain morphology, phase transformation, microstructural coarsening, and also in mechanical properties. Furthermore, high cooling rates generate non-equilibrium microstructures which, depending on the processed material and on the specific application, may require a post-thermal treatment (Ref 17).

As material melting based processes are regarded, SLM is one of the most utilized processes because of the relatively low cost and high parts performances and surface finishing (Ref 18). The main SLM process parameters, usually considered to optimize the process, are laser power, beam size, scanning speed, scanning strategy, hatch spacing, layer thickness, and powder particle size. A key role in the optimization of the AM process is played by building direction and the related choice of support structures that are critical to successfully build a part (Ref 19, 20, 21).

Yan et al. (Ref 22) studied the effect of the building directions on surface macro/micro- structure and tribological properties of Inconel 625 samples manufactured by SLM with directions 0°, 45°, 90°. They found fine microstructure and a large number of equiaxed grains in the SLM 0° sample, while coarse microstructure and reduced quantity of equiaxed grains were observed in the SLM 45° sample. Sun et al. (Ref 23) studied the effects of build direction (0°, 45° and 90°) on tensile and fatigue performance of Ti6Al4V manufactured by the selective laser melting technique. They found that the build direction has a slight effect on tensile strength and ductility. The tensile strengths of the 0° and 90° resulted in the minimum and maximum ultimate tensile stress, respectively. In detail, they found that the UTS of 0° specimens is equal to 935 MPa and UTS of 90° specimens is equal to 953 MPa. Furthermore, they found that the building direction has a significant influence on fatigue performance of SLM Ti6Al4V products. Fatigue strength of the 0° and the 90° specimen at 10^7 cycles was found equal to 300 MPa and 350 MPa, respectively. Finally, they highlight that voids, porosities and unmelted powders were the main reasons for low ductility and poor fatigue performance in the material. Xie et al (Ref 24) analyzed effects of build direction, 0° sample, 90° sample, on the tensile and microstructural properties of material. They found that different build orientations and dimensions of the part being built induce different cooling rates during the SLM process and a SLM build orientation along the length direction of Ti–6Al–4V alloy benefits the production of a final material with better overall mechanical performance. Major findings include that the 90° sample has a larger elongation value and better plasticity than the 0° sample. Furthermore the 90° sample showed an UTS equal to 1065 MPa, while the 0° sample an UTS equal to 1236 MPa. The amount of martensite phase was evaluated finding that lower α/α' ratio and α'' phase result in higher tensile strength and lower plasticity. Similar trends were reported also in (Ref 25, 26). Hartunian et al. (Ref 27) also studied the effect of build orientation on the microstructure and mechanical properties of Ti–6Al–4V specimens manufactured by selective laser melting. The tensile test revealed lower yield, ultimate tensile strength and strain in the samples printed in the Z orientation (90°) with brittle planar fracture features perpendicular to the build direction.

From the microstructural point of view, it has to be noticed that during the process the rapid heating and melting of powder layers promote the epitaxial β grains growth and therefore result in elongated grains of β phase in the building direction (Ref 28). After the rapid solidification, proper of SLM process, β grains are transformed into α' metastable martensite, with hierarchical structure α' (α', α'', α''') (Ref 29, 30, 31), surrounded by the original β grains edge (Ref 32, 33). The above-described morphology is typical of surfaces parallel to the building direction. Instead, in surfaces orthogonal to the building direction, near-equiaxic morphology of the martensite α' phase, delimited by original grain edge of the β phase before the fast cooling, can be observed. The typical microstructure of these surfaces also allows to highlight the used scanning strategy.

Although a few researches have focused on the effect of the building orientation on the main metallurgical and mechanical properties of the final parts, the above-described SoA shows contrasting results, indicating that a clear understanding of the complex thermo-mechanics of the process and occurring microstructural evolutions has not been fully achieved. As for similar building direction conflicting results, namely in terms of elongation and UTS, are present in the literature, it can be inferred that experimental results should better highlight the effects of the building direction on the main factors affecting the overall part performances, i.e., microstructure evolution and integrity.

In this paper, the effects of build direction on microstructure evolution, micro defects and micro-mechanical performances of selective laser melted Ti6Al4V parts were highlighted, as a function of the "building direction", in order to find a key to reading for the apparently discordant data present in the literature. Two build direction samples (0°, 90°) were manufactured and analyzed using optical metallographic microscope (OM) and scanning electron microscopy (SEM). The influencing factors for the heterogeneity in the microstructure, as grain morphology, defects, phase transformation, and microstructural coarsening were investigated by isometric microstructure reconstruction in the three orthogonal planes for each sample. The correlation between micro-mechanical performances and microstructure of the SLM samples was investigated by microhardness tests.

2. Materials and Methods

The used Ti6Al4V alloy is a material characterized by high strength, excellent biocompatibility and low density and the typical microstructure of kind α + β. Considering that during the SLM process rapid cooling leads to the formation of very fine acicular metastable martensite α', the material obtained at the end of the process is characterized by high strength and low ductility.

2.1 Building Parameters and Scan Strategy

The SLM specimens were produced using SLM 280HL machine with set parameters chosen as subsequently reported: laser power 350 W, scanning speed 1400 mm/s, hatch distance 120 μm, layer thickness 30 μm, argon atmosphere. During the process, the build platform was maintained at 200° C. The used scanning strategy consists of parallel linear trajectories tilted at 45°, with respect to the reference axes of the base plate, which are rotated 90° for each subsequent layer. Figure 1 shows the
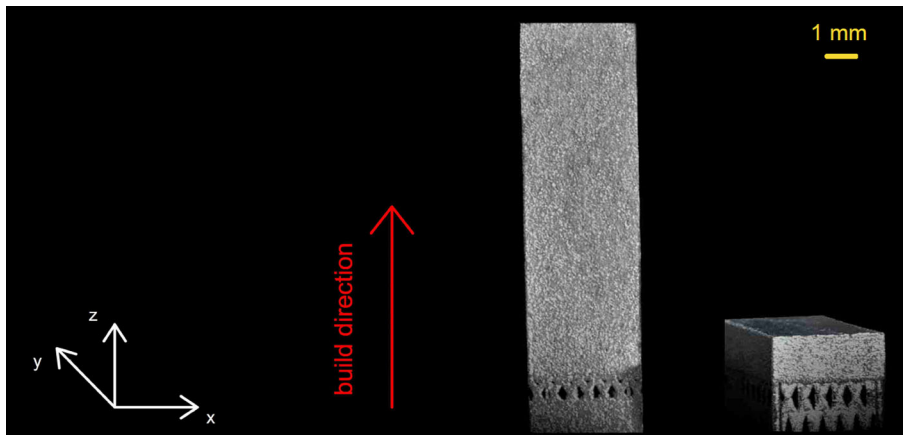
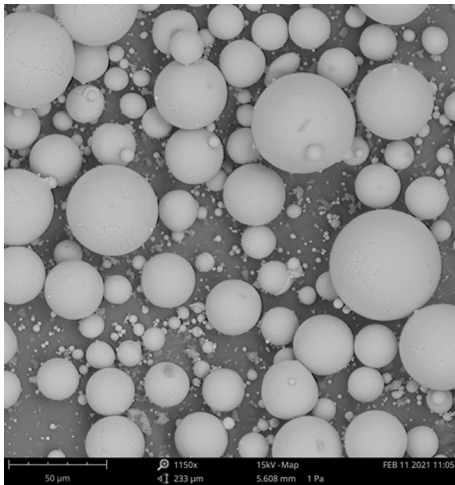**Fig. 1** Build direction of samples 90°(left) and 0° (right)

Fig. 2 SEM image of the Ti-6Al-4V used Gaussian powder with size between 20 and 60 μm

produced samples with the indication of reference axes and angles.

2.2 Powder

The used Ti6Al4V powder is a typical Gaussian powder with size between 20 and 60 μm. Figure 2 shows the SEM image of the used powder from which the above average dimensionality has been evaluated.

2.3 Specimen Characterization

The influencing factors for the heterogeneity in the microstructure, i.e., grain morphology, phase transformation, microstructural coarsening and defects, including the evaluation of the average porosity, where present, were investigated by isometric microstructure reconstruction in the three orthogonal planes for each sample. The correlation between micro-mechanical performances and microstructure of the SLM samples was investigated by microhardness tests. The characterization of the samples, according to the stratification directions of the material, was carried out in terms of three-dimensional analysis of the microstructure of the processed material using an Olympus GX 51 optical microscope. Phenom ProX Desktop was used for the SEM analyses. The micro

mechanical characterization of the material, in terms of microhardness, was carried out on a Remet HBV 30 and correlated to the previous analyses. The obtained results were correlated to the thermal gradients relative to the SLM process in the two different configurations and specific material heterogeneity factors were identified.

Standard metallographic procedures as grounding and polishing were used to prepare the metallographic samples. Subsequently the specimens were etched using Kroll's Reagent for 35 s to reveal the microstructure. In order to carry out the microstructural, porosity and microhardness analyses and to highlight any heterogeneity of the specimens produced in the two configurations, the volume of each sample, of size of 10 $\times$ 4 $\times$ 25 mm, was divided into four zones, as shown in Fig. 3. In the four zones the microstructural properties, in terms of morphology and average grain dimension, and the mechanical characteristics, in terms of microhardness, were evaluated in three orthogonal planes consisting of the front, side and cross-sectional faces of the sample. The purpose of this choice was to assess the heterogeneity of these characteristics within the same part.

Both for the evaluation of the average grain dimension and for the evaluation of the average microhardness (Vickers microhardness tests performed using a weight of 1000 g), seven measurements were carried out for the front and cross-sectional surfaces and five for the lateral surfaces. A similar assessment of seven measurements on the front and cross-sectional surfaces and five measurements on lateral surfaces were carried out to assess the mean porosity of each surface in each zone (i.e. 1, 2, 3, 4).

3. Results and Discussion

3.1 Microstructural Analysis

The grain morphology and microstructural coarsening, which are key influencing factors for the heterogeneity of the microstructure, were investigated by isometric microstructure reconstruction in the three orthogonal planes for each sample and with reference to each of the zones above highlighted. The results of the microstructural analysis are shown in Fig. 4 and 5, for the morphological study, and in Tables 1 and 2 reporting the average grain dimension. The typical microstructure of these
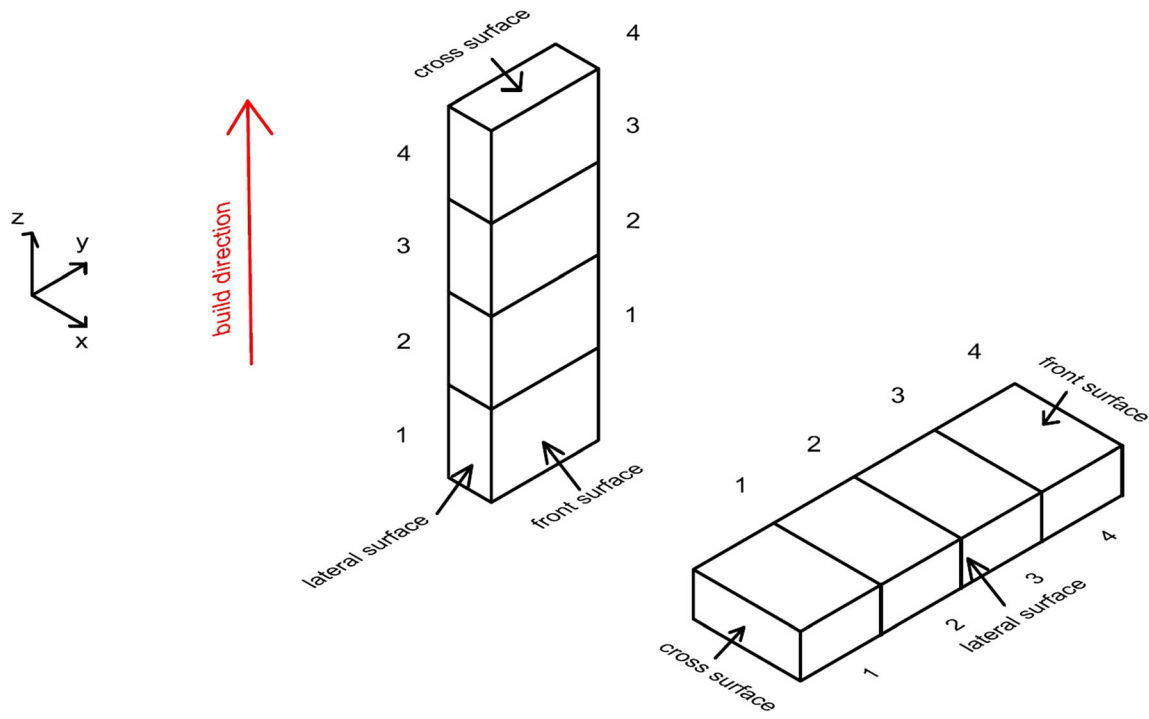
Fig. 3 The four zones utilized for microstructural and porosities analysis
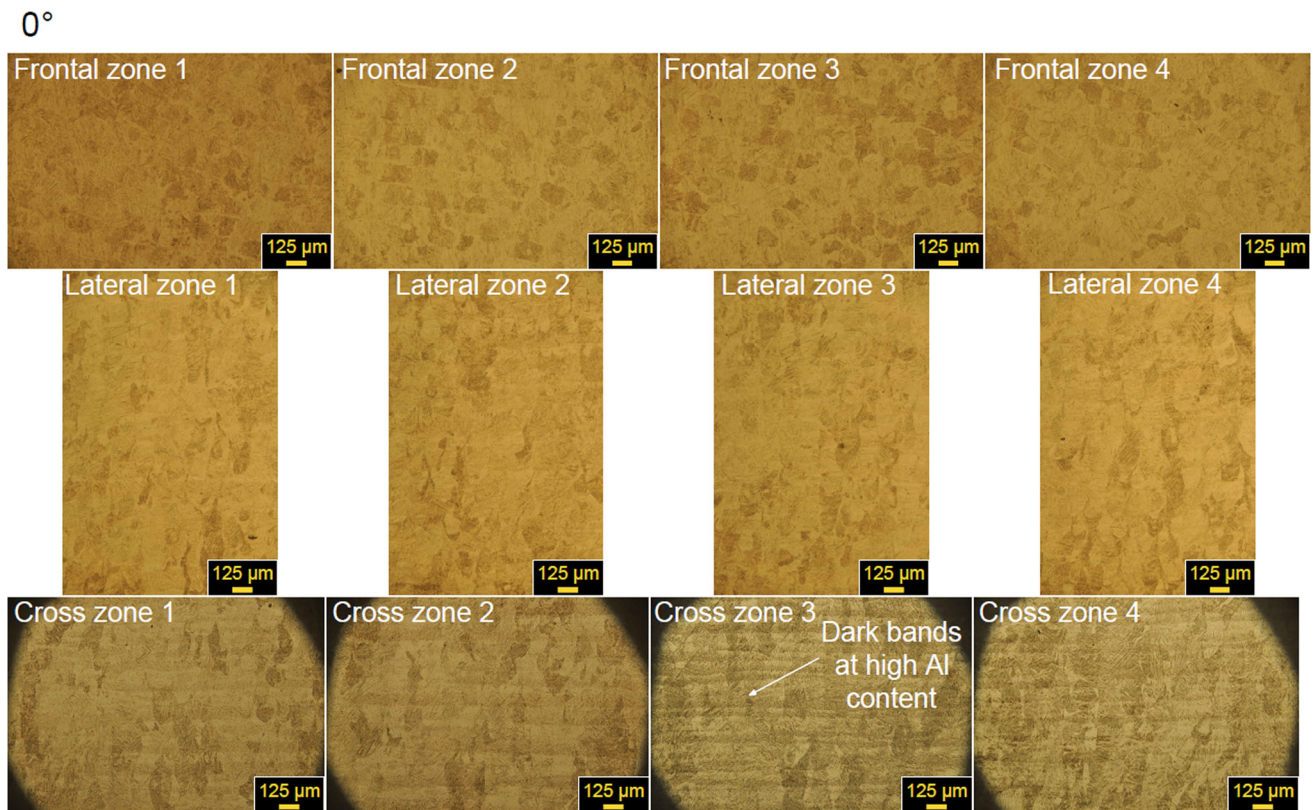

Fig. 4 Microstructural analysis of the specimen made by SLM process 0° building direction after 35 s chemical etching with Kroll's Reagent

surfaces also allows to highlight the used scanning strategy. In the two cases covered in this paper, 0° and 90°, the surfaces with near-equiaxic morphology are, respectively, the frontal and transverse surfaces.

The dimensional assessments carried out in terms of the average size of the austenitic β grains within which, as a result of rapid cooling, the martensitic phase α' is formed, with possible hierarchical structure (α'', α''', α''''), are closely
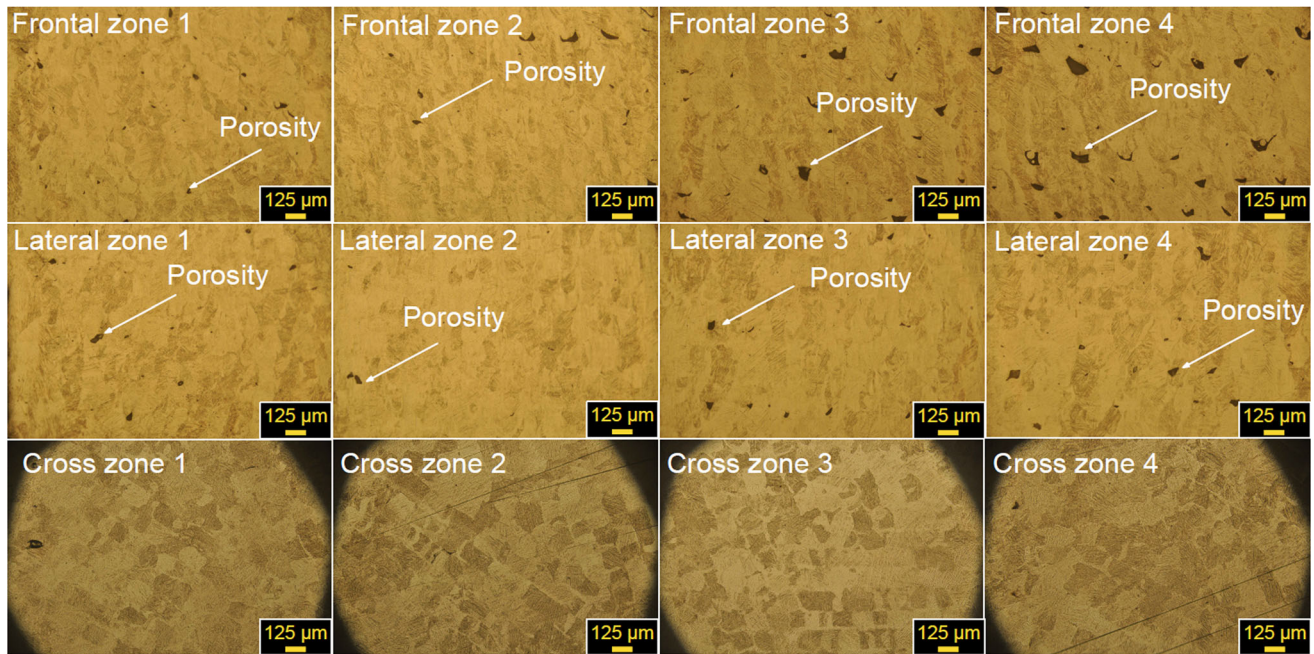
90°

Fig. 5 Microstructural analysis of the specimen made by SLM process 90° building direction after 35 s chemical etching with Kroll's Reagent

Table 1   Average grain dimensions in 0° building direction samples

0°	Frontal surface Average grain dimension, μm	Lateral surface average epitaxial grain dimension [large-long], μm	Cross surface average epitaxial grain dimension [large-long], μm
Zone 1	95 (σ = 12)	95 (σ = 12)–420 (σ = 21)	95 (σ = 12)–420 (σ = 21)
Zone 2	108 (σ = 8)	108 (σ = 8)–310 (σ = 18)	108 (σ = 8)–310 (σ = 18)
Zone 3	125 (σ = 10)	125 (σ = 10)–300 (σ = 6)	125 (σ = 10)–300 (σ = 6)
Zone 4	130 (σ = 6)	130 (σ = 6)–400 (σ = 12)	130 (σ = 10)–400 (σ = 12)

Table 2   Average grain dimensions in 90° building direction samples

90°	Frontal surface average epitaxial grain dimension [large-long], μm	Lateral surface average epitaxial grain dimension [large-long], μm	Cross surface Average grain dimension, μm
Zone 1	128 (σ = 6)–400 (σ = 20)	128 (σ = 6)–380 (σ = 22)	125 (σ = 5)
Zone 2	126 (σ = 8)–410 (σ = 18)	126 (σ = 8)–320 (σ = 18)	130 (σ = 7)
Zone 3	130 (σ = 12)–480 (σ = 16)	129 (σ = 12)–320 (σ = 15)	124 (σ = 12)
Zone 4	127 (σ = 15)–480 (σ = 20)	127(σ = 15)–400 (σ = 22)	124 (σ = 15)

related to the average size of the α' phase since the length of the plates of the aforementioned phase is delimited by the size of the original β austenitic grain.

The three-dimensional reconstruction analysis of the microstructure of material subjected to the SLM process made it possible to evaluate the morphology and average grain size in each surface, frontal, lateral and transversal, in the different zones and to correlate the obtained dimensional results with the thermal flows typical of each of the two configurations (90° e 0°).

The average grain size was calculated using the intercept technique and therefore a line was drawn though each micrograph at 100X. The number of grain boundaries, intersecting the aforementioned line, was counted and the average

grain size was found by dividing the number of intersections by the actual line length.

Larger surfaces allow higher thermal flows that may promote finer microstructure. In detail, it was noted that for the 0° case study there is a progressive increase in the average grain size in the longitudinal direction of the specimens, i.e., from the zone 1 toward the zone 4. This longitudinal lack of homogeneity is directly related to the scanning strategy. In fact, in this case, the strategy used promotes decreasing thermal gradients along the longitudinal direction of the specimen. In the transverse sections of the samples, from which it is possible to observe the different stratifications, dark bands are visible, revealing the melt pool boundaries in each layer. In particular, these dark bands are less pronounced in zone 1 of the sample,

the one first deposited in each layer, and become more pronounced and thicken toward zones 3 and 4, which are those deposited last. In zone 3, marked dark bands were observed. The above-mentioned morphology confirms the presence of decreasing thermal gradients from the zone 1 toward the zone 4 and also the minimum of thermal gradients is reached in zone 3. In zone 4, although still affected by reduced thermal gradients, thinner and less marked dark bands are observed, as this is the last deposited area. The formation of such bands is related to the small sample size along the production direction. Finally, it should be noted that, although the thickening of dark bands in zone 3 is an indication of low thermal gradients and therefore slower cooling, resulting in larger average grain size and consequently lower microhardness values, these areas are characterized by microhardness values higher with respect to the adjacent zones. This is because, as several authors have outlined, a high Al content is found in the dark bands, which leads to the formation of Ti_3Al precipitated contributing to increase microhardness (Ref 15, 34). A quantitative analysis of the Ti3Al precipitates should be carried out with a TEM (Ref 35) which was not available for this research.

For the case study obtained with building direction of 90°, it should be highlighted that the small deposited area coupled with a large number of deposited layers observed in zone 1 indicates that the material in this zone remains at high temperatures for the longest times. Starting from a qualitative evaluation of the heat flux based on the part geometry and the build orientation, it can be stated that, although zones 2, 3 and 4 remain at high temperatures for lower times, thermal gradients are reduced along the stratification direction, i.e., the material cools down more slowly. These phenomena result in slight variations in the average grain size in the different zones. However, the numerical values, shown in Table 2, suggest that there is a trend of progressive decrease in the average size of the grain from zone 1 to zone 4. In other words, the effects of permanence time at high temperatures prevail over the ones of

reducing thermal gradients along the longitudinal direction of the specimens. On the contrary, the reduction of thermal gradients along the longitudinal directions prevails in zone 3, which results in an increase in the average grain size, although this zone remains at high temperatures for a shorter time than zone 1 and 2.

3.2 Porosity Evaluation

Porosities were measured by using the software Matlab Image analysis toolbox applied on micrographic acquired images. Such method discriminates the dense regions (light zones) with pores and defects (dark areas). Taking advantage of the considerable contrast between porosity and the microstructure of the material, it is possible to apply the threshold techniques that allow to obtain a binary image. The binarization process allows to distinguish and compute the percentage of porosity defect: dense regions are colored with white; instead, pores and defects are colored with dark. Finally, the software computes the area fraction of dark area (corresponding to pores). In the study, after performing the binarization of the image with the porosity represented in black and the microstructure represented in white, for a better visualization, the binarization map was reversed, thus obtaining the porosities represented in white and the microstructure in black (Fig. 6).

Therefore, the porosity evaluation was based on planimetric methods using a suitable software (Matlab Image Analysis), inside on, a subroutine for the three-ortogonal reconstruction of porosity has been defined.

The microstructural analysis highlighted that only for build orientation of 90° porosity defect is found, while no porosity was found in the 0° oriented specimens. In Fig. 7 a micrographic SEM image of porosity defect, due to lack of fusion, found in the 90° samples is reported.

In order to assess the porosity index for each area, i.e., the percentage of volume occupied by porosity in the different areas, the threshold analysis above described was carried out on
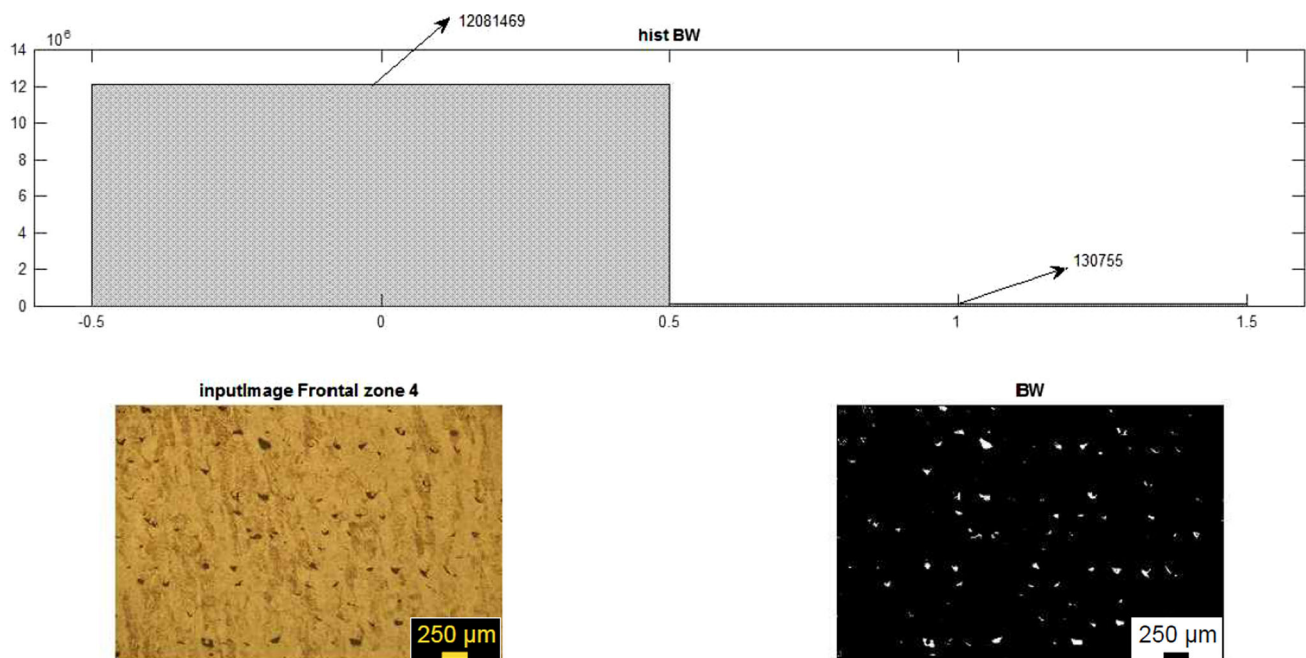

Fig. 6 Image analysis for volume porosity quantification

the micrographs acquired for the frontal, lateral and transverse surfaces of each area.

An index of porosity (Ip) of each zone was calculated as the product of the porosity percentage on each surface (front, lateral and cross) for the extent of the same surface (front 62,5 mm^2, lateral 25 mm^2 and cross 40 mm^2) and the result was divided for the volume of single zone of specimen (250 mm3). In this way, the index (Ip) provides an estimate of the average porosity percentage in the volume and therefore allows to highlight heterogeneity in the distribution of these types of defects within each sample. In this way, the estimate of porosity, in terms of volumetric percentages within the volume characteristic of each of the four considered zones (Fig. 3), was calculated using the weighted sum, mediated in the volume of each area, of the surface porosity in the three orthogonal surfaces.

The accuracy of this estimation technique has been verified by comparing the estimated porosity values with those found in the literature with reference to similar material subjected to SLM (Ref 36, 37, 15) finding porosity values consistent with the values here estimated.

The obtained results, summarized in Table 3, show the presence of a low porosity, i.e., 0,19 %, in the first layers of the sample which increases up to 0,31 % in the direction of sample stratification, i.e., building direction. This result is linked to the fact that, due to the small surface worked for each individual layer, the thermal gradients between the deposited layer and the already solidified material are decreasing as processing progresses (Ref 38). As the thermal gradient decreases, the time of stay in the liquid phase of each individual layer increases, and therefore, the phenomenon of balling effect, which is responsible for the formation of porosity, is promoted.
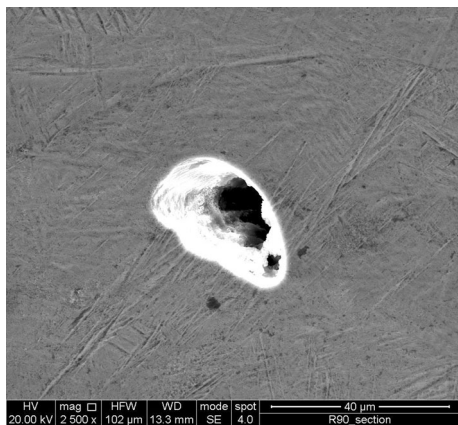

Fig. 7 SEM image of pore in a cross surface of 90° building direction specimen

A similar porosity trend (porosity increasing with layers) was also found in (Ref 39). However, in the above cited paper only the overall average porosity was given losing the detailed analysis of the effect of building direction on the variation of porosity inside the specimen. On the contrary, in this study, the measuring campaign was aimed to identify a trend along the building direction and to appreciate the effect of the heat accumulation that occurs in the 90° specimen.

Finally, it is highlighted that in the 0° building direction, although a decrease in thermal gradients has been observed in the longitudinal direction of the sample, the larger surface dimension ensures the establishment of sufficient thermal gradients to avoid the balling effect.

3.3 Microhardness Evaluation

The correlation between micro-mechanical performances and microstructure of the SLM samples was investigated by microhardness tests. In each of the zones considered for the previous analyses the average HV value was determined and the results are summarized in Fig. 8.

For the 0° sample it is observed a progressive reduction in microhardness values from the zone 1 toward the zone 4. These reductions are more marked in larger areas and become smaller in smaller areas.

In the transverse surface, the less extended surface, the aforementioned phenomenon results less evident. It is noted that in the latter surface there is an out-of-trend microhardness value (408 HV) in the zone 3. This last value is related to the presence in this area of dark bands with a high aluminum content, in which Ti$_3$Al precipitates are formed. These results confirm that the 0° configuration is the one that involves the highest thermal flows and therefore the cooling of the material is faster. The thermal flow is also facilitated by the presence of a wide distribution of supports at the base of the specimens.

For the 90° sample a progressive increase in microhardness values from the zone 1 toward the zone 4 is observed, being the increase is more marked in larger areas and smaller in smaller areas. This trend confirms the prevalence of the material softening phenomenon due to the time of permanence at high temperatures. As indicated above, this phenomenon is more significant in zone 1, gradually decreasing in zones 2, 3 and 4. The out-of-trend microhardness values, observed in zone 3 of both the frontal surface and the cross surface and in zone 2 of the transverse surface, are linked to the phenomenon of thermal gradients decreasing along the building direction that prevails over the softening phenomenon in the opposite direction to the building one (Ref 40). It is worth noting that the observed HV trends are consistent with what found, for both the orientations considered, in terms of the average grain size. In particular, with finer grain size higher values of microhardness are
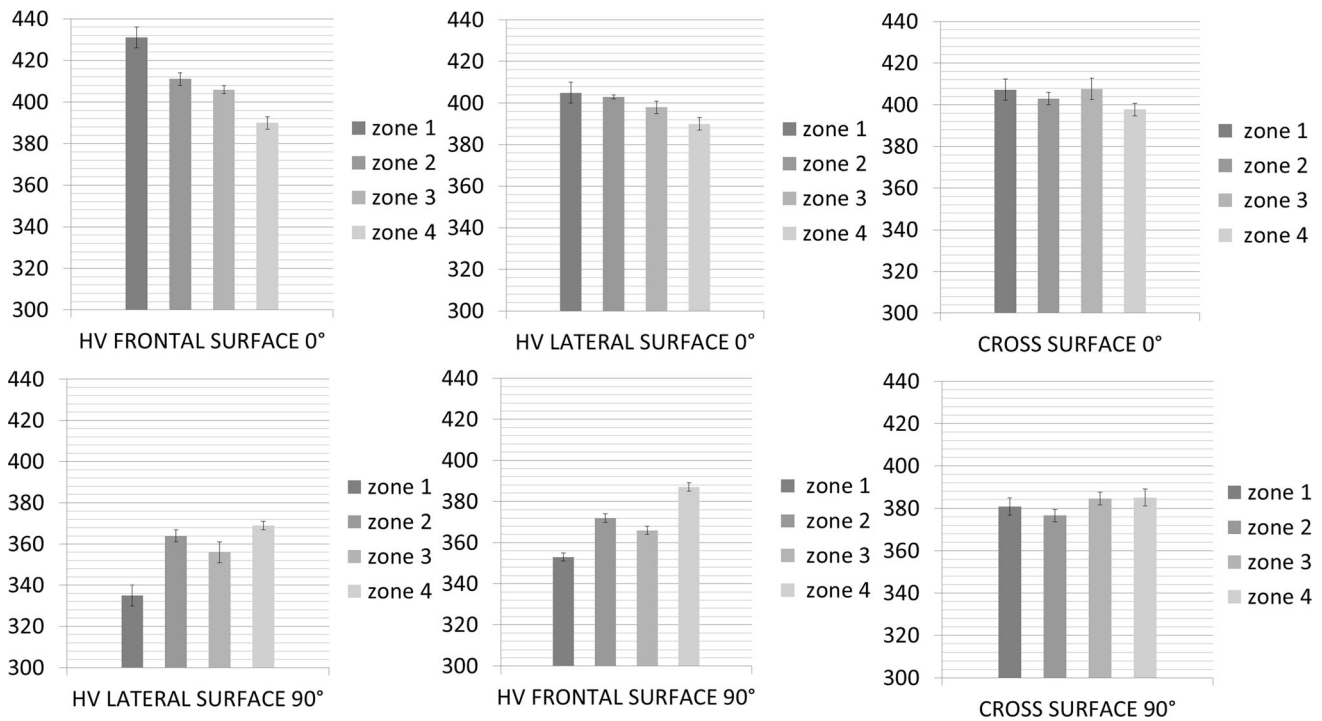
Table 3 Porosity evaluation results

	Frontal surface porosity, %	Lateral surface porosity, %	Cross surface porosity, %	Ip, %
Zone 1	0.71	0.11	0.01	**0.19**
Zone 2	0.67	0.16	0.05	**0.19**
Zone 3	1.19	0.16	0.08	**0.31**
Zone 4	1.08	0.28	0.09	**0.31**

Fig. 8 Average microhardness in zones 1, 2, 3, 4 for each configuration (0° and 90°) in the frontal, lateral and cross surface

detected, while decreasing microhardness values have been observed as the average grain size increases.

Finally, it is noted that for the configuration 0° higher microhardness values than those found in the samples in the 90° configuration are obtained.

It is worth observing that, although the obtained values are within the ranges of the values found in literature (Ref 36), a direct comparison cannot be carried out as, to the author knowledge, no paper focused on the variation of microhardness within a given specimen due to the building direction.

4. Conclusions

The effect of the building directions, 0° and 90°, on the microstructure evolutions and microhardness properties of SLM Ti6Al4V samples were studied. Main conclusions from this study are as follows:

- Small sample sizes in the building direction cause low thermal gradients and therefore slower cooling that promote the formation of dark bands with a high aluminum content that may lead to the formation of Ti_3Al precipitates, resulting in longitudinal lack of homogeneity of the mechanical and microstructural properties of the final part. In fact, the decreasing trend in longitudinal direction of microhardness values produced by the increasing of average grain dimension is interrupted by an out-of-trend microhardness value due to the presence of Ti3Al precipitates.
- Small deposited surface coupled with a high number of deposited layers (90°) generate a material softening in the direction opposite to the building one, due to the increasing of the permanence time at high temperature, coupled

with a local softening in the zone 3. In this zone the softening phenomenon due to the reduction in thermal gradients along the building direction is predominant.

- Small deposition surfaces, such as in the 90° samples, also facilitate the reduced thermal gradients between the different layers. As a consequence, the heterogeneous formation of porosity, increasing along the building direction, is promoted. Hence, it can be stated that the orientation of the sample, directly affecting the size of the material surface deposited in each layer, for a given specimen geometry, can be considered a main factor for the formation of porosity.
- Higher microhardness values are obtained in configuration 0°, in each zone, than those found in the samples in the 90° configuration because of the presence of high thermal flows resulting in faster cooling of the material.
- The greater microstructural heterogeneity observed in the 0° sample was related to the scanning strategy. On the other hand, porosities were found in the 90° sample and were related to the reduction of thermal gradients toward the building direction and the reduced size of the surface deposited in each layer.

Literature studies, relating to the effect of the building direction on the properties of the Ti6Al4V alloy subjected to SLM, contain conflicting results in relation to the same building orientation value. This required a study aimed to identifying building orientation-related factors that could justify the apparent discrepancies between the literature results. The microstructure and microhardness analyses carried out, as well as porosity, made it possible to highlight the type and thermal flows according to the size of the deposited surface together with the number of deposited layers. Thermal storage factors and form factors that need to be considered jointly with the building direction have been highlighted.

Overall, the obtained results indicate that the building direction plays a key role on the mechanical properties of the produced parts as it has a strong influence on the thermal gradient, which, in turn, affects average grain size, porosities and microhardness. However, for a given building direction, also the dimensions of the produced parts, and hence of the deposited surface, affects the thermal gradients, being the latter higher with larger surfaces. These two phenomena, if correlated, can explain the apparently discordant data present in the literature.

The obtained results can be used as guidelines for the design of more complex geometries in order to determine the most appropriate object positioning on the base plate as related to the final part mechanical properties and workability during finishing operations.

Funding

Open Access

References

1. J.P. Oliveira, T.G. Santos and R.M. Miranda, Revisiting Fundamental Welding Concepts to Improve Additive Manufacturing: From Theory to Practice, *Prog. Mater. Sci.*, 2020, **107**, p 100590. https://doi.org/10.1016/j.pmatsci.2019.100590

2. J.P. Oliveira, A.D. LaLonde and J. Ma, Processing Parameters in Laser Powder Bed Fusion Metal Additive Manufacturing, *Mater. Des.*, 2020, **193**, p 1–12.

3. F.F. Conde, J.D. Escobar, J.P. Oliveira, A.L. Jardini, W.W. Bose Filho and J.A. Avila, Austenite Reversion Kinetics and Stability during Tempering of an Additively Manufactured Maraging 300 Steel, *Addit. Manuf.*, 2019, **29**, p 100804. https://doi.org/10.1016/j.addma.2019.100804

4. F.F. Conde, J.D. Escobar, J.P. Oliveira, M. Béreš, A.L. Jardini, W.W. Bose and J.A. Avila, Effect of Thermal Cycling and Aging Stages on the Microstructure and Bending Strength of a Selective Laser Melted 300-Grade Maraging Steel, *Mater. Sci. Eng. A*, 2019, **758**, p 192–201.

5. N. Raghavan, S. Simunovic, R. Dehoff, A. Plotkowski, J. Turner, M. Kirka and S. Babu, Localized Melt-Scan Strategy for Site Specific Control of Grain Size and Primary Dendrite Arm Spacing in Electron Beam Additive Manufacturing, *Acta Mater.*, 2017, **140**, p 375–387. https://doi.org/10.1016/j.actamat.2017.08.038

6. J. Raplee, A. Plotkowski, M.M. Kirka, R. Dinwiddie, A. Okello, R.R. Dehoff and S.S. Babu, Thermographic Microstructure Monitoring in Electron Beam Additive Manufacturing, *Sci. Rep.*, 2017, **7**(1), p 1–16.

7. T.A. Rodrigues, V.R. Duarte, D. Tomás, J.A. Avila, J.D. Escobar, E. Rossinyol and J.P. Oliveira, In-Situ Strengthening of a High Strength Low Alloy Steel during Wire and Arc Additive Manufacturing (WAAM), *Addit. Manuf.*, 2020, **34**, p 101200. https://doi.org/10.1016/j.addma.2020.101200

8. J.G. Lopes, C.M. Machado, V.R. Duarte, T.A. Rodrigues, T.G. Santos and J.P. Oliveira, Effect of Milling Parameters on HSLA Steel Parts Produced by Wire and Arc Additive Manufacturing (WAAM), *J. Manuf. Process.*, 2020, **59**, p 739–749. https://doi.org/10.1016/j.jmapro.2020.10.007

9. P.K. Gokuldoss, S. Kolla and J. Eckert, Additive manufacturing processes: Selective laser melting, electron beam melting and binder jetting—Selection guidelines, *Mater. (Basel)*, 2017, **10**(6), p 672.

10. C.Y. Yap, C.K. Chua, Z.L. Dong, Z.H. Liu, D.Q. Zhang, L.E. Loh and S.L. Sing, Review of Selective Laser Melting: Materials and Applications, *Appl. Phys. Rev.*, 2015 https://doi.org/10.1063/1.4935926

11. W.E. Frazier, Metal Additive Manufacturing: A Review, *J. Mater. Eng. Perform.*, 2014, **23**(6), p 1917–1928.

12. X. Chen, K. Liu, W. Guo, N. Gangil, A.N. Siddiquee and S. Konovalov, The Fabrication of NiTi Shape Memory Alloy by Selective Laser Melting: A Review, *Rapid Prototyp. J.*, 2019, **25**(8), p 1421–1432.

13. K.C. Chang, J.R. Zhao and F.Y. Hung, Microstructure, Mechanical Properties, and Fatigue Fracture Characteristics of High-Fracture-Resistance Selective Laser Melting Al-Ni-Cu Alloys, *Metals (Basel)*, 2021, **11**(1), p 1–13.

14. G.P. Toker, M. Nematollahi, S.E. Saghaian, K.S. Baghbaderani, O. Benafan, M. Elahinia and H.E. Karaca, Shape Memory Behavior of NiTiHf Alloys Fabricated by Selective Laser Melting, *Scr. Mater.*, 2020, **178**, p 361–365.

15. L. Thijs, F. Verhaeghe, T. Craeghs, J. Van Humbeeck and J.P. Kruth, A Study of the Microstructural Evolution during Selective Laser Melting of Ti-6Al-4V, *Acta Mater.*, 2010, **58**(9), p 3303–3312.

16. M. Iebba, A. Astarita, D. Mistretta, I. Colonna, M. Liberini, F. Scherillo, C. Pirozzi, R. Borrelli, S. Franchitti and A. Squillace, Influence of Powder Characteristics on Formation of Porosity in Additive Manufacturing of Ti-6Al-4V Components, *J. Mater. Eng. Perform.*, 2017, **26**(8), p 4138–4147.

17. A.M. Beese, Microstructure and Mechanical Properties of AM Builds. *Thermo-Mechanical Model. Addit. Manuf* 2018, p 81–92

18. Y. Zhang, L. Wu, X. Guo, S. Kane, Y. Deng, Y.G. Jung, J.H. Lee and J. Zhang, Additive Manufacturing of Metallic Materials: A Review, *J. Mater. Eng. Perform.*, 2018, **27**(1), p 1–13.

19. H.K. Rafi, N.V. Karthik, H. Gong, T.L. Starr and B.E. Stucker, Microstructures and Mechanical Properties of Ti6Al4V Parts Fabricated by Selective Laser Melting and Electron Beam Melting, *J. Mater. Eng. Perform.*, 2013, **22**(12), p 3872–3883.

20. Y. Kok, X.P. Tan, P. Wang, M.L.S. Nai, N.H. Loh, E. Liu and S.B. Tor, Anisotropy and Heterogeneity of Microstructure and Mechanical Properties in Metal Additive Manufacturing: A Critical Review, *Mater. Des.*, 2018, **139**, p 565–586.

21. S. Liu and Y.C. Shin, Additive Manufacturing of Ti6Al4V Alloy: A Review, *Mater. Des.*, 2019, **164**, p 8–12.

22. X. Yan, S. Gao, C. Chang, J. Huang, K. Khanlari, D. Dong, W. Ma, N. Fenineche, H. Liao and M. Liu, Effect of Building Directions on the Surface Roughness, Microstructure, and Tribological Properties of Selective Laser Melted Inconel 625, *J. Mater. Process. Technol.*, 2020, **2021**, p 288.

23. W. Sun, Y. Ma, W. Huang, W. Zhang and X. Qian, Effects of Build Direction on Tensile and Fatigue Performance of Selective Laser Melting Ti6Al4V Titanium Alloy, *Int. J. Fatigue*, 2019, **2020**, p 130.

24. Z. Xie, Y. Dai, X. Ou, S. Ni and M. Song, Effects of Selective Laser Melting Build Orientations on the Microstructure and Tensile Performance of Ti–6Al–4V Alloy, *Mater. Sci. Eng. A*, 2020, **776**, p 139001. https://doi.org/10.1016/j.msea.2020.139001

25. C. Qiu, N.J.E. Adkins and M.M. Attallah, Microstructure and Tensile Properties of Selectively Laser-Melted and of HIPed Laser-Melted Ti-6Al-4V, *Mater. Sci. Eng. A*, 2013, **578**, p 230–239.

26. M. Simonelli, Y.Y. Tse and C. Tuck, Effect of the Build Orientation on the Mechanical Properties and Fracture Modes of SLM Ti-6Al-4V, *Mater. Sci. Eng. A*, 2014, **616**, p 1–11. https://doi.org/10.1016/j.msea.2014.07.086

27. P. Hartunian and M. Eshraghi, Effect of Build Orientation on the Microstructure and Mechanical Properties of Selective Laser-Melted Ti-6Al-4V Alloy, *J. Manuf. Mater. Process.*, 2018, **2**(4), p 69.

28. S.Q. Wu, Y.J. Lu, Y.L. Gan, T.T. Huang, C.Q. Zhao, J.J. Lin, S. Guo and J.X. Lin, Microstructural Evolution and Microhardness of a Selective-Laser-Melted Ti-6Al-4V Alloy after Post Heat Treatments, *J. Alloys Compd.*, 2016, **672**, p 643–652.

29. G.M. Ter Haar and T.H. Becker, Selective Laser Melting Produced Ti-6Al-4V: Post-Process Heat Treatments to Achieve Superior Tensile Properties, *Mater. (Basel)*, 2018, **11**(1), p 146.

30. J.J.S. Dilip, S. Zhang, C. Teng, K. Zeng, C. Robinson, D. Pal and B. Stucker, Influence of Processing Parameters on the Evolution of Melt Pool, Porosity, and Microstructures in Ti-6Al-4V Alloy Parts Fabricated by Selective Laser Melting, *Prog. Addit. Manuf.*, 2017, **2**(3), p 157–167.

31. J. Yang, H. Yu, J. Yin, M. Gao, Z. Wang and X. Zeng, Formation and Control of Martensite in Ti-6Al-4V Alloy Produced by Selective Laser Melting, *Mater. Des.*, 2016, **108**, p 308–318.

32. J. Irwin, Modeling Microstructure of AM Processes Using the FE Method, *Thermo-Mech. Model. Addit. Manuf.*, 2017 https://doi.org/10.1016/B978-0-12-811820-7.00009-4

33. H. Ali, H. Ghadbeigi and K. Mumtaz, Processing Parameter Effects on Residual Stress and Mechanical Properties of Selective Laser Melted Ti6Al4V, *J. Mater. Eng. Perform.*, 2018, **27**(8), p 4059–4068. https://doi.org/10.1007/s11665-018-3477-5

34. B. Vrancken, L. Thijs, J.P. Kruth and J. Van Humbeeck, Heat Treatment of Ti6Al4V Produced by Selective Laser Melting: Microstructure and Mechanical Properties, *J. Alloys Compd.*, 2012, **541**, p 177–185.

35. H. Wu, G. Fan, L. Geng, X. Cui and M. Huang, Nanoscale Origins of the Oriented Precipitation of Ti3Al in TiAl Systems, *Scr. Mater.*, 2016, **125**, p 34–38. https://doi.org/10.1016/j.scriptamat.2016.07.037

36. G. Kasperovich and J. Hausmann, Improvement of Fatigue Resistance and Ductility of TiAl6V4 Processed by Selective Laser Melting, *J. Mater. Process. Technol.*, 2015, **220**, p 202–214.

37. J. Mezzetta, J.P. Choi, J. Milligan, J. Danovitch, N. Chekir, A. Bois-Brochu and M. Brochu, Microstructure-Properties Relationships of Ti-6Al-4V Parts Fabricated by Selective Laser Melting, *Int. J. Precis. Eng. Manuf.-Green Technol.*, 2018, **5**(5), p 605–612.

38. C. Phutela, N.T. Aboulkhair, C.J. Tuck and I. Ashcroft, The Effects of Feature Sizes in Selectively Laser Melted Ti-6Al-4V Parts on the Validity of Optimised Process Parameters, *Mater. (Basel)*, 2020, **13**(1), p 117.

39. S. Ren, Y. Chen, T. Liu and X. Qu, Effect of Build Orientation on Mechanical Properties and Microstructure of Ti-6Al-4V Manufactured by Selective Laser Melting, *Metall. Mater. Trans. A Phys. Metall. Mater. Sci.*, 2019, **50**(9), p 4388–4409.

40. G.E. Bean, T.D. McLouth, D.B. Witkin, S.D. Sitzman, P.M. Adams and R.J. Zaldivar, Build Orientation Effects on Texture and Mechanical Properties of Selective Laser Melting Inconel 718, *J. Mater. Eng. Perform.*, 2019, **28**(4), p 1942–1949. https://doi.org/10.1007/s11665-019-03980-w